BIOCHEMISTRY
including biophysical chemistry & molecular biology
Article

Biochemistry **2010,** *49,* 4027–4035 4027
DOI: 10.1021/bi100155j

Thermodynamics and Kinetics of Association of Antibiotics with the Aminoglycoside Acetyltransferase (3)-IIIb, a Resistance-Causing Enzyme†

Adrianne L. Norris,‡ Can Özen,§ and Engin H. Serpersu*,‡,∥

‡*Department of Biochemistry and Cellular and Molecular Biology, The University of Tennessee, Knoxville, Tennessee 37996,* §*Department of Biotechnology and Central Laboratory Molecular Biology and Biotechnology R&D Center, Middle East Technical University, Ankara, Turkey, and* ∥*Graduate School of Genome Science and Technology, The University of Tennessee and Oak Ridge National Laboratories, Knoxville, Tennessee 37996, and Bioscience Division, Oak Ridge National Laboratory, Oak Ridge, Tennessee 37831*

Received February 1, 2010; Revised Manuscript Received April 9, 2010

ABSTRACT: The thermodynamic and kinetic properties of interactions of antibiotics with the aminoglycoside acetyltransferase (3)-IIIb (AAC) are determined with several experimental methods. These data represent the first such characterization of an enzyme that modifies the 2-deoxystreptamine ring common to all aminoglycoside antibiotics. Antibiotic substrates for AAC include kanamycin A, kanamycin B, tobramycin, sisomicin, neomycin B, paromomycin, lividomycin A, and ribostamycin. Kinetic studies show that kanamycin group aminoglycosides have higher k_{cat} values than members of the neomycin group. Only small aminoglycosides without intraring constraints show substrate inhibition. Isothermal titration calorimetry (ITC) and fluorescence measurements are consistent with a molecular size-dependent stoichiometry where binding stoichiometries are 1.5−2.0 for small antibiotics and 1.0 for larger. Antibiotic−enzyme interaction occurs with a favorable enthalpy ($\Delta H < 0$) and a compensating unfavorable entropy ($T\Delta S < 0$). The presence of coenzyme A significantly increases the affinity of the antibiotic for AAC. However, the thermodynamic properties of its ternary complexes distinguish this enzyme from other aminoglycoside-modifying enzymes (AGMEs). Unlike other AGMEs, the enthalpy of binding becomes more favored by 1.7−10.0-fold in the presence of the cosubstrate CoASH, while the entropy becomes 2.0−22.5-fold less favored. The overall free energy change is still only 1.0−1.9 kcal/mol from binary to ternary for all antibiotics tested, which is similar to those for other aminoglycoside-modifying enzymes. A computationally derived homology model provides structural support for these conclusions and further indicates that AAC is likely a member of the GCN5-related acetyltransferase family of proteins.

Pathogenic bacteria are emerging with increasing levels of resistance to clinically used aminoglycoside antibiotics. While several resistance mechanisms have been observed, the most prominent is the enzymatic covalent modification of the antibiotic in which aminoglycosides are a target in both Gram-positive and Gram-negative bacteria. Enzymes used for this purpose can serve as *N*-acetyltransferases (AAC),[1] *O*-phosphotransferases (APH), or *O*-nucleotidyltransferases (ANT) which transfer an acetyl, phosphate, or nucleotide moiety, respectively, from a bound coenzyme. An aminoglycoside with even one of these chemical modifications has a significant loss of affinity for the bacterial ribosome where it would normally bind and interfere with protein translation (*1*, *2*). Moreover, each of these transferase families contains members that modify different positions on the antibiotics. Bacteria often harbor genes that encode more than one of these enzymes, thus complicating treatment of infections (*3*).

To date, our laboratory has used a variety of biophysical methods to characterize the thermodynamic properties of enzyme−ligand complexes of a representative from both the phosphotransferase and nucleotidyltransferase families, namely, APH (3′)-IIIa and ANT (2″)-Ia (*4*−*9*). These enzymes not only catalyze different reactions but also modify rings A and C of aminoglycosides (*4*−*9*) (Figure 1). This paper introduces the aminoglycoside acetyltransferase (3)-IIIb (AAC) and describes the first detailed characterization of an enzyme responsible for modifying the 3-N position on the central 2-deoxystreptamine ring (2-DOS) (Figure 1, ring B). This specificity heralds special importance since all typical aminoglycosides contain an amine substituent at carbon 3 of the 2-DOS ring, and any modification of this site causes the loss of antibiotic effectiveness (*10*). Here, the substrate profiles and general properties of binding to aminoglycosides in various binary and ternary complexes using isothermal titration

†This work is supported by a grant from the National Science Foundation (MCB-0842743 to E.H.S.) and by the Hunsicker Award (to E.H.S.) through the Department of Biochemistry and Cellular and Molecular Biology at The University of Tennessee. A.L.N. is partly supported by the Department of Energy EPSCoR Implementation Award (DE-FG02-08ER46528).

*To whom correspondence should be addressed: Walters Life Sciences Bldg. M407, The University of Tennessee, Knoxville, TN 37996-0840. Telephone: (865) 974-2668. Fax: (865) 974-6306. E-mail: serpersu@utk.edu.

[1]Abbreviations: APH (3′)-IIIa, aminoglycoside phosphotransferase (3′)-IIIa; ANT (2″)-Ia, aminoglycoside nucleotidyltransferase (2″)-Ia; AAC, aminoglycoside acetyltransferase (3)-IIIb; GNAT, GCN5-related acetyltransferase; IPTG, isopropyl β-D-1-thiogalactopyranoside; PMSF, phenylmethanesulfonyl fluoride; Tris-HCl, 2-amino-2-(hydroxymethyl)-propane-1,3-diol hydrochloride; PIPES, piperazine-1,4-bis(2-ethanesulfonic acid); HEPES, 4-(2-hydroxyethyl)-1-piperazineethanesulfonic acid; ACES, 2-(carbamoylmethylamino)ethanesulfonic acid; 2-DOS, 2-deoxystreptamine; AG, aminoglycoside; AGME, aminoglycoside-modifying enzyme; AcCoA, acetyl coenzyme A; CoASH, coenzyme A; ITC, isothermal titration calorimetry; BLAST, Basic Local Alignment Search Tool; COBALT, Constraint-based Multiple Alignment Tool.

Published on Web 04/13/2010

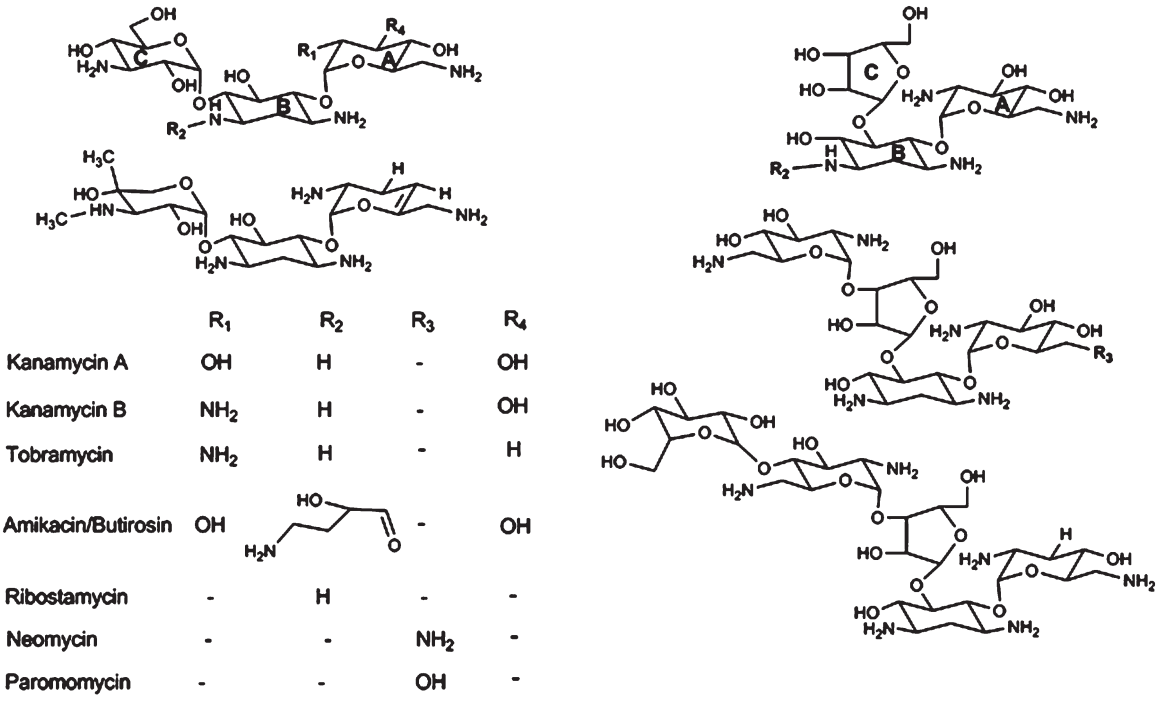

FIGURE 1: Aminoglycoside structures. The 2-deoxystreptamine ring (ring B) is 4,6-disubstituted in the kanamycin class (left), while neomycin class (right) aminoglycosides are 4,5-disubstituted. Note that amikacin and butirosin are in the kanamycin and neomycin classes, respectively. The five-ring antibiotic shown is lividomycin A, while the structure containing a double bond in ring A is sisomicin.

calorimetry (ITC) and intrinsic tryptophan fluorescence are outlined. A homology structure of AAC was also determined to aid interpretation of experimental data; the structure also suggests that AAC is another member of the GNAT superfamily of acetyltransferases.

EXPERIMENTAL PROCEDURES

Chemicals and Reagents. Butirosin was the generous gift of D. Baker (The University of Tennessee). High-performance Ni-Sepharose resin was purchased from Amersham Biosciences (Piscataway, NJ), while IPTG was obtained from Inalco Spa (Milan, Italy). Ion exchange matrix, Macro Q, was purchased from Bio-Rad Laboratories (Hercules, CA). Purified thrombin was graciously provided by E. Fernandez (The University of Tennessee). All other aminoglycosides, coenzymes, and reagents were purchased at the highest possible purity from Sigma.

Cloning, Overexpression, and Purification of AAC. Previously in our laboratory, AAC (3)-IIIb (henceforth to be called AAC for the sake of simplicity except in cases where clarification necessitates) was cloned and purified from inclusion bodies (*11*). Enzyme isolated in this way, however, was not amenable to many biophysical and spectroscopic studies. Therefore, the AAC gene was cloned with an N-terminal, six-His tag and thrombin cleavage site from the original *Pseudomonas aeruginosa* plasmid [provided by G. Miller (Achaogen) and K. Shaw (formerly of Schering Plough)] (*11*) and transformed into *Escherichia coli* BL21(DE3) cells for overexpression in a soluble form. *E. coli* TOP10 cells were used for long-term storage of the plasmid.

Overexpression began by inoculation of 1 mL of Luria broth (LB) containing 0.1 mg/mL ampicillin (amp) with an isolated colony grown on LB agar plates (0.1 mg/mL amp). After growing for 12 h, the bacteria were transferred to 200 mL of LB with 0.1 mg/mL amp and grown for 18−24 h; 35 mL of this culture was then transferred to 800 mL of LB with 0.05 mg/mL amp and grown to an optical density of ~1.0 at 600 nm. AAC expression was then induced by addition of IPTG to a final concentration of 1 mM. All steps in the overexpression protocol were performed at 37 °C. Cells were harvested after induction for 4 h and stored at −80 °C. The protein was found to remain stable in cells stored at this temperature for more than 12 months.

For purification, BL21 cells were taken from storage, suspended in lysis buffer [100 mM NaCl, 20 mM imidazole, 200 μM PMSF, and 50 mM Tris-HCl (pH 7.6) at 4 °C], and lysed with three passes through a French press. Crude lysate was then loaded onto a 1 mL Ni-Sepharose column. After extensive column washing using 100 mM NaCl, 20 mM imidazole, and 50 mM Tris-HCl (pH 7.6) at 4 °C, AAC was eluted with an imidazole gradient from 100 to 350 mM. AAC consistently eluted in fractions containing between 140 and 250 mM imidazole. After this step, SDS−PAGE analysis showed AAC to be >99% pure. Furthermore, the ratio of the UV absorbance at 280 and 260 nm was >1.6, ensuring sufficient freedom from nucleic acids. The protein solution was then dialyzed against 100 mM NaCl and 50 mM Tris-HCl (pH 7.6) at 4 °C to remove imidazole and excess salt. To avoid interference from the six-His tag, 200 μL of thrombin per 25 mg of AAC was incubated at 25 °C for 1 h. The protein solution was then passed through a Ni-Sepharose column to remove the free His tag. Cleavage was observed to be >90% as most AAC eluted from the Ni^{2+} affinity column during the loading and washing steps. Because isoelectric points of AAC and thrombin differ by >3 pH units, ion exchange chromatography was utilized to remove the protease. Finally, the AAC solution was dialyzed extensively against the appropriate buffer at 50 mM (pH 7.6) at 4 °C and 100 mM NaCl. Final protein yields were consistently between 15 and 20 mg/L of induced culture. The concentration of AAC was determined spectrophotometrically using an $\varepsilon^{0.1\%}$(280 nm) of 1.4.

Fluorescence Spectroscopy. The change in intrinsic tryptophan fluorescence intensity was used to detect interactions of antibiotics with AAC using a Perkin-Elmer (Boston, MA) model

LS 55 fluorescence spectrometer equipped with a stirred four-position cell changer with a 1 cm light path. Excitation occurred at 295 nm, while emission was monitored at 345 nm. Sample solutions contained 1 μM AAC, 100 mM NaCl, and 50 mM Tris-HCl (pH 7.6) at 25 °C. Titrations of aminoglycosides were conducted via addition of 1−5 μL of concentrated, serially diluted stocks into a sample volume of 2.5 mL to a maximum sample dilution of 2.4%. To obtain dissociation constants (K_D), the percent change in fluorescence intensity was plotted versus substrate concentration and saturation curves were fit to the single-site binding equation:

$$(\Delta F/F_0) \times 100 = [(\Delta F/F_0) \times 100][S]/(K_D + [S]) \quad (1)$$

where $(\Delta F/F_0) \times 100$ is the percent change in fluorescence intensity and F_0 represents the fluorescence intensity of the sample prior to addition of substrate. Titrations of antibiotics yielded an increase in fluorescence intensity. Aminoglycoside titrations into buffer did not yield any change in the fluorescence signal.

Isothermal Titration Calorimetry (ITC). ITC experiments were performed on a VP-ITC microcalorimeter from Microcal, Inc. (Northampton, MA), at 25 °C. AAC concentrations were between 10 and 40 μM for the maintenance of *c* values ([binding sites] × association constant) within the range of 1−100 for greater accuracy of association constant (K_A) measurements. Desulfated aminoglycosides (*12*) were present in the syringe at concentrations ranging from 13 to 60 times greater than that of AAC in the cell. Substrates were diluted into the final dialysis buffer used in enzyme purification, allowing both cell and syringe solutions to contain 100 mM NaCl and the appropriate buffer at 50 mM (pH 7.6) at 25 °C. In ternary experiments, CoASH was included in the cell solution at a first site saturating concentration while the antibiotic was titrated from the syringe. Samples were degassed for 10 min prior to being loaded. Titrations of ligands into buffer were performed as a control, and the resulting heats of ligand dilution were subtracted from the experimental data prior to curve fitting. The pH of each cell and syringe solution was checked before and after each experiment, and no change was observed. The integrity of AAC was ensured by measurement of the enzymatic activity and concentration before and after each experiment. In all cases, the enzymatic activity remained greater than 87% of the starting activity at the end of titrations. Thermograms were integrated using Origin software provided by the instrument manufacturer, and the best fits were obtained with one-site binding. Since binding of aminoglycosides to the enzyme causes shifts in the pK_a values of several functional groups, all titrations were performed individually in Tris-HCl, HEPES, and PIPES buffers with heats of ionization (ΔH_{ion}) of 11.4, 5.02, and 2.74 kcal/mol, respectively, to determine the intrinsic enthalpy (ΔH_{int}) as described below. ΔG values were calculated from association constants (K_A) derived from fitted titration curves using the equation $\Delta G = -RT \ln(K_A)$. $T\Delta S$ values were then determined from the relationship $\Delta G = \Delta H_{int} - T\Delta S$.

Data from the three buffers described above were used to construct a plot of the observed heat, ΔH_{obs}, versus ΔH_{ion} which yields a linear correlation of the equation $\Delta H_{obs} = (\Delta n)(\Delta H_{ion}) + \Delta H_{int}$, where Δn is the net number of protons transferred as a result of ligand binding and ΔH_{int} is the intrinsic enthalpy of binding. This equation is the simplified form of the equation $\Delta H_{obs} = \Delta H_{int} + \Delta n[\alpha\Delta H_{ion} + (1 - \alpha)\Delta H_{enz}] + \Delta H_{bind}$. ΔH_{obs} denotes the observed binding enthalpy of formation of a complex in a given buffer, where ΔH_{ion} describes the heat of ionization of the buffer. The term $\Delta n[\alpha\Delta H_{ion} + (1 - \alpha)\Delta H_{enz}]$ represents the heat of ionization of groups from the ionization of buffer and the protein to maintain pH, where α represents the fraction of protonation contributed by the buffer (*13*). In addition, ΔH_{bind} represents the heat of binding of buffer to the enzyme. In the presence of high salt (i.e., 100 mM NaCl), ΔH_{bind} is assumed to be zero and the contribution from the ionization of amino acids remains the same at a given pH. Thus, by performing experiments in buffers with different heats of ionization, one can easily determine ΔH_{int} and Δn. However, note that ΔH_{int} still includes the heat of ionization of groups from protein and ligand that are contributing to Δn which would represent the true ΔH_{int} only when $\Delta n = 0$. For the buffers used in this work, a net proton uptake by the enzyme−ligand complex yields a positive Δn. In the case of binary titrations with kanamycin A, ACES (ΔH_{ion} = 7.5 kcal/mol) replaced Tris-HCl because its heat of ionization almost completely masked ITC signals for this experiment.

Titrations of neomycin into the AAC−CoASH complex yielded a dissociation constant in the submicromolar range, making the *c* value > 300. Protein concentrations could not be decreased to lower the *c* value because of enzyme instability under dilute conditions. To obtain a more accurate dissociation constant (K_D) for dissociation of neomycin from the ternary AAC−CoASH−neomycin complex, we performed the following experiment. The cell was loaded with AAC in complex with a first site saturation level of CoASH and enough ribostamycin to saturate > 95% of the binding sites. Neomycin was loaded into the syringe and subsequently titrated into the AAC−CoASH−ribostamycin complex. Because the dissociation constants of neomycin and ribostamycin differ by 1 order of magnitude, the latter serves as a competitive inhibitor against neomycin. From the fit of this titration curve, the apparent dissociation constant [$K_{D(app)}$] was obtained (Figure S1 of the Supporting Information) and used to determine the dissociation constant for neomycin.

Steady State Kinetics. Kinetic parameters were determined by a continuous assay using a Cary-Win UV−vis spectrophotometer (Varian, Palo Alto, CA). The following coupled reaction allowed AAC activity to be monitored via the increasing absorbance of pyridine 4-thiolate at 324 nm (*14*):

$$\begin{aligned} &AG + AcCoA \xrightarrow{AAC} AG\text{-}C(O)CH_3 + CoASH \\ &4,4'\text{-dipyridyl disulfide} + CoASH \rightarrow CoA\text{-}S\text{-}S\text{-pyridine} \\ &\qquad + \text{pyridine 4-thiolate} \end{aligned} \quad (I)$$

Samples consisted of 100 mM NaCl and 50 mM Tris-HCl (pH 7.6) at 25 °C. AAC (10 nM) was used in each assay, and the reaction was initiated by addition of aminoglycoside at various concentrations while the AcCoA concentration was held at 100 μM. The signal molecule, 4,4′-dipyridyl disulfide, was present in excess at 750 μM. Reactions followed Michaelis−Menten type kinetics with all substrates tested. Since substrate inhibition, as in several aminoglycoside-modifying enzymes, is observed with AAC, reported kinetic parameters were determined via fits of specific activity (micromoles per minute per milligram) versus substrate concentration to the equation

$$v = \frac{V_{max}[S]}{K_m + [S] + [S]^2/K_i} \quad (2)$$

where *v* is the initial velocity, V_{max} is the maximal velocity, K_m is the Michaelis constant, and K_i is the substrate inhibition

Table 1: Kinetic Parameters for Antibiotics[a]

substrate	K_m (μM)	V_{max} (μmol min^{-1} mg^{-1})	k_{cat} (s^{-1})	k_{cat}/K_m ($\times 10^6$ M^{-1} s^{-1})	K_i (μM)
neomycin B	1.2 ± 0.2	18.4 ± 3.4	9.5 ± 1.8	9.1 ± 3.6	> 1500
paromomycin	3.3 ± 0.6	65.0 ± 2.7	33.6 ± 1.4	10.8 ± 2.5	> 500
ribostamycin	2.3 ± 0.6	45.6 ± 5.3	23.5 ± 2.7	10.6 ± 1.7	59.4 ± 17.2
lividomycin A	3.6 ± 0.1	65.5 ± 2.7	33.8 ± 1.4	9.5 ± 0.8	> 600
kanamycin A	4.8 ± 0.5	99.4 ± 8.6	51.4 ± 4.4	11.2 ± 2.3	381 ± 95
kanamycin B	2.6 ± 1.6	105 ± 7.0	54.5 ± 3.6	34.4 ± 19.8	26.3 ± 18.6
tobramycin	1.3 ± 0.8	92.5 ± 9.3	47.8 ± 4.8	60.5 ± 34.6	17.3 ± 5.9
sisomicin	1.5 ± 0.4	89.6 ± 4.3	46.3 ± 2.2	33.4 ± 9.5	> 700

[a]Data and errors are calculated from the average of two trials, with errors being the standard error of the mean.

Table 2: ITC-Derived Thermodynamics of Aminoglycoside Binding[a]

aminoglycoside	N	K_D (μM)	ΔH_{int} (kcal/mol)	$-T\Delta S$ (kcal/mol)	ΔG (kcal/mol)	Δn
NeoB Bin	1.1 ± 0.04	0.6 ± 0.1	−16.3 ± 2.1	7.8 ± 1.0	−8.5 ± 0.1	0.6 ± 0.2
NeoB Tern	1.1 ± 0.1	0.04 ± 0.02[c]	−28.5 ± 3.1	18.5 ± 2.0	−9.9 ± 0.2	0.8 ± 0.2
Paro Bin	1.0 ± 0.02	9.2 ± 0.4	−18.4 ± 0.9	11.5 ± 0.6	−6.9 ± 0.04	1.1 ± 0.1
Paro Tern	0.9 ± 0.01	1.5 ± 0.3	−32.7 ± 2.6	24.7 ± 2.0	−8.0 ± 0.1	1.9 ± 0.3
Ribo Bin	1.8 ± 0.1	53.3 ± 5.5	−6.8 ± 0.4	0.9 ± 0.1	−5.8 ± 0.1	0.4 ± 0.02
Ribo Tern	0.9 ± 0.1	4.7 ± 0.9	−27.5 ± 0.7	20.2 ± 0.5	−7.3 ± 0.1	1.1 ± 0.4
KanA Bin	2.7 ± 0.3	79.8 ± 22.9	−1.2 ± 0.4	−4.4 ± 1.3	−5.6 ± 0.2	−0.07 ± 0.07
KanA Tern	1.7 ± 0.3	16.0 ± 1.4	−12.8 ± 1.3	6.2 ± 0.6	−6.6 ± 0.1	1.3 ± 0.3
KanB Bin	1.6 ± 0.2	29.5 ± 2.2	−8.1 ± 0.5	1.9 ± 0.1	−6.2 ± 0.04	0.6 ± 0.01
KanB Tern	1.0 ± 0.8	3.9 ± 0.8	−26.0 ± 0.5	18.6 ± 0.4	−7.4 ± 0.1	1.5 ± 0.03
Tobr Bin	1.5 ± 0.1	33.4 ± 7.0	−8.4 ± 0.8	2.3 ± 0.2	−6.2 ± 0.1	0.6 ± 0.1
Tobr Tern	1.1 ± 0.02	2.9 ± 0.6	−22.2 ± 1.7	14.6 ± 1.1	−7.6 ± 0.1	1.0 ± 0.1
Amik Tern[b]	1.9 ± 0.1	101 ± 4.1	−7.7 ± 0.5	2.2 ± 0.1	−5.5 ± 0.4	not determined
Buti Tern[b]	2.2 ± 0.2	165 ± 15	−5.7 ± 0.7	0.6 ± 0.1	−5.1 ± 0.6	not determined

[a]Given errors are calculated as the standard error of the mean of two to six trials. Errors in the intrinsic enthalpy (ΔH_{int}) and in net protonation (Δn) are derived from the deviation from linearity of ΔH_{obs} vs ΔH_{ion} curves. Bin and Tern refer to the binary and ternary complexes as per the absence or presence of CoASH with AAC, respectively. [b]These experiments were performed only in PIPES buffer (pH 7.6) at 25 °C and 100 mM NaCl. [c]The dissociation constant for the neomycin ternary complex was determined via competition with ribostamycin as described in Experimental Procedures.

constant. Turnover rates (k_{cat}) were calculated from the relationship $V_{max} = k_{cat}[E]_T$.

Computation of the AAC Homology Model. The amino acid sequence of AAC was submitted to several homology modeling servers available online via Expasy protein databank (http://ca.expasy.org/tools), including EsyPred3D (*15*), SWISS-MODEL (*16*−*18*), and Geno3d (*19*). All yielded two proteins, Yokd and AAC (3) from *Bacillus* [Protein Data Bank (PDB) entries 2NYG and 3IJW, respectively], as the top hits. Each resulting model was further energy minimized and analyzed with Molecular Operating Environment (MOE) (*20*). From these, that of the SWISS-MODEL, which used Yokd (chain A) as the template, had the fewest ϕ and ψ angle outliers (10) and steric clashes (11) and contained all residues except the first three of the N-terminus and the last six of the C-terminus. Therefore, this model is used to aid in interpretation of some of the experimental data.

RESULTS AND DISCUSSION

Kinetic Specificity with Aminoglycosides. Steady state kinetic analysis reveals that tobramycin, kanamycin A, kanamycin B, sisomicin, neomycin B, paromomycin A, ribostamycin, and lividomycin (Figure 1) are all substrates with measurable rates. Although low micromolar K_m values of all tested aminoglycosides are within a narrow range (Table 1), catalytic turnover rates (k_{cat}) reveal that the kanamycin class aminoglycosides are bound, acetylated, and released more quickly than members of the neomycin class (Table 1). While k_{cat} values for kanamycin group aminoglycosides are between 46 and 55 s^{-1}, the range for members of the neomycin group covers values between 10 and 34 s^{-1}. To the best of our knowledge, this is the first observation of such discrimination among those aminoglycoside-modifying enzymes that can use both kanamycins and neomycins as substrates. This suggests that antibiotic orientation in the active site, governed by the 4,5- or 4,6-substitution pattern on the 2-deoxystreptamine ring (2-DOS) (Figure 1), plays a role in how fast AAC is able to function. An interesting observation was that neomycin B exhibited a significantly lower k_{cat} even compared to the rest of the neomycin group aminoglycosides. Aminoglycosides substituted at the N-1 site (amikacin and butirosin) do not show any measurable rates even when a high concentration of enzyme is present. Turnover rates are estimated to be less than 7.7×10^{-4} and 8.3×10^{-6} s^{-1} for amikacin and butirosin, respectively. Since these antibiotics can still bind to the enzyme (Table 2), apparently the presence of any bulky group at N-1 distorts the orientation of the antibiotic in the active site such that N-3 cannot be aligned optimally for acetylation regardless of the substitution pattern of the 2-deoxystreptamine ring.

Specificity constants (k_{cat}/K_m) for the reaction catalyzed by AAC are on the order of 10^7 M^{-1} s^{-1} for the vast majority of aminoglycosides, a value that ranks among the highest of all aminoglycoside-modifying enzymes studied to date (*21*−*26*). Despite the antibiotic-specific differences in K_m, k_{cat} compensates in most cases, the result being that all specificity constants fall within a narrow range (Table 1). However, those antibiotics in

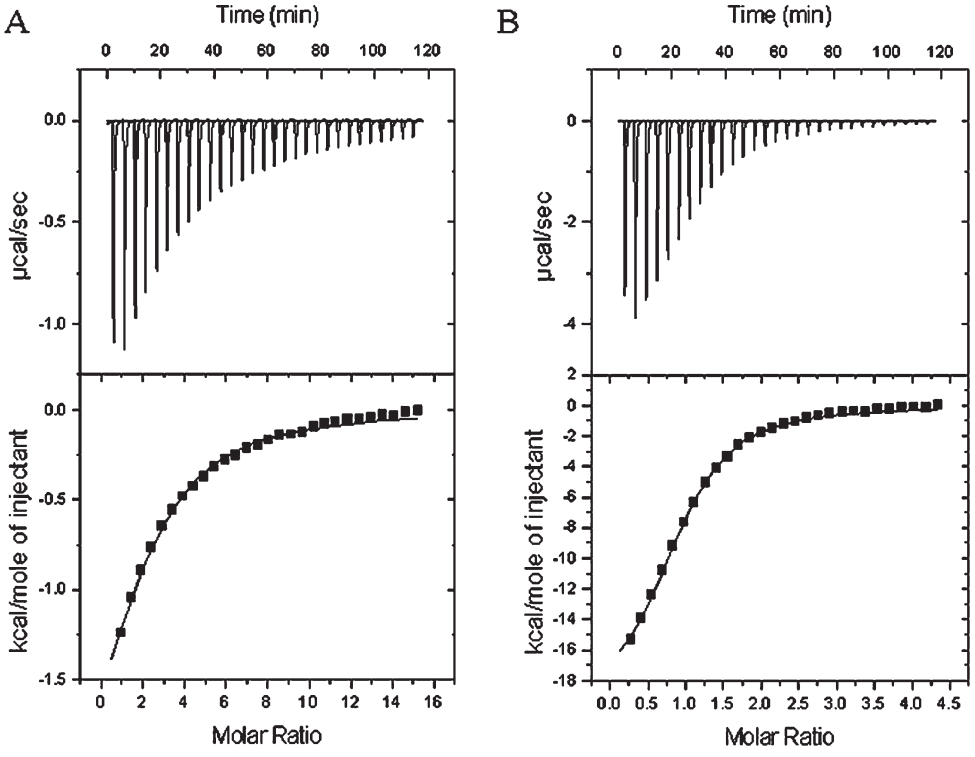

FIGURE 2: Typical ITC signals for the titration of an antibiotic into AAC. (A) Typical thermogram (top) and isotherm (bottom) of the titration of an antibiotic into AAC. In the isotherm, data points are shown with a fitted line to single-site binding. (B) Titration of the same antibiotic into the AAC−CoASH complex illustrating the increase in heat and affinity from the significant changes in both *x* and *y* axis scales.

the kanamycin class that have a 2′-amine group (tobramycin, kanamycin B, and sisomicin) have higher specificity constants than the rest.

Like those for many other AGMEs, high concentrations of antibiotics induce substrate inhibition of AAC activity. K_i and K_m values are not correlated, meaning that a given antibiotic with a low K_m does not necessarily exhibit a low K_i. However, we observed that the smaller and/or less structurally constrained aminoglycosides, including kanamycin B, ribostamycin, and tobramycin, have significantly stronger inhibition constants than those larger than them or those with a more conformationally restricted ring structure (i.e., lividomycin or sisomicin, respectively).

Antibiotic Binding. Binding of several aminoglycosides with a 4,5- and 4,6-disubstituted 2-DOS ring to AAC was studied by fluorescence and ITC to determine the thermodynamic properties of AAC−ligand complexes. While ITC studies form the main source of thermodynamic data, dissociation constants and stoichiometries of enzyme−ligand complexes determined by fluorescence were in excellent agreement with those from ITC.

Thermodynamic studies of only a select few aminoglycoside-modifying enzymes can be found in the literature (*6*−*9*, *27*). Among these, it has been shown that antibiotic binding occurs with a favorable enthalpy ($\Delta H < 0$) and a compensating unfavorable entropy ($T\Delta S < 0$), yielding a net result of a favorable ΔG. The same is true of AAC−aminoglycoside interactions in which binding of aminoglycosides to AAC is an exothermic reaction (Figure 2) accompanied by negative entropy (Table 2), with the possible exception of kanamycin A where the formation of the binary complex occurs with a favorable entropic contribution. We should note, however, that the binding of kanamycin A to AAC occurs with a very small heat release (the directly measured quantity in ITC) with the weakest binding constant compared to those of all substrates of this enzyme. Thus, these data may be more prone to curve fitting errors because of the low signal-to-noise ratio.

The general trends of favorable ΔH and unfavorable $T\Delta S$ for AGME−antibiotic associations hold regardless of whether the cofactor(s) is present. However, there is a difference between AAC and the other AGMEs. Data acquired with enzymes that utilize MgATP as a cosubstrate, APH (3′)-IIIa and ANT (2″)-Ia, show that the presence of a metal-ATP analogue at saturating concentrations induces a less favorable intrinsic enthalpy and a more favorable entropy for antibiotic association relative to those in the absence of the analogue as observed with APH (3′)-IIIa (*7*). In the case of ANT (2″)-Ia, some aminoglycosides show the same pattern as APH (3′)-IIIa while others have no significant change from binary to ternary (*9*). For APH (3′)-IIIa, this phenomenon is attributed in part to hydrogen bond breakage in a β-sheet as a result of nucleotide binding (*4*). The only other aminoglycoside acetyltransferase with available thermodynamic data is the aminoglycoside acetyltransferase (6′)-Iy [AAC (6′)-Iy]. With these, enzyme data for both binary and ternary complexes were acquired with only one aminoglycoside, lividomycin, and showed that neither ΔH, $T\Delta S$, nor ΔG is altered in the presence of a cofactor (*27*). In contrast to these observations, ΔH becomes 1.7−10.0-fold more favorable in the presence of CoASH (Figures 2 and 3) while $T\Delta S$ is 2.0−22.5-fold less favorable for binding of aminoglycosides to AAC (Table 2). The net result is a small change in the overall free energy (ΔG) for the formation of the ternary complex which becomes more favorable by only 1.0−1.9 kcal/mol relative to the binary complex. Among the enzymes with data available, AAC is the only one that modifies the 2-DOS ring. Thus, our data suggest that the observed difference in thermodynamics of enzyme−ligand complexes is more dependent on the site of modification than the type of reaction catalyzed by AGMEs. Data from multiple enzymes are needed to confirm this observation.

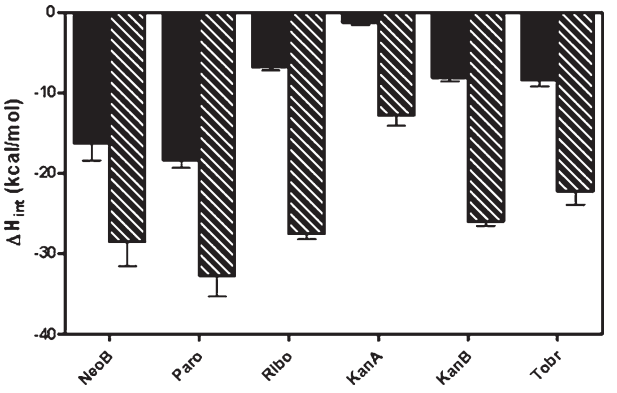

FIGURE 3: Intrinsic enthalpy for binding of an antibiotic to AAC. The intrinsic enthalpy of antibiotic binding is much more favorable in the presence of CoASH. Here, the solid bars represent binary titrations of antibiotic into AAC while striped bars are titrations into the AAC in a complex with a saturating level of CoASH.

The weakened entropic contribution in the titration of the AAC−CoASH complex with antibiotics may be due to cofactor stabilization of a particular protein conformational state in which certain loops are positioned for optimal aminoglycoside binding. In the absence of CoASH, the equilibrium may be shifted toward a conformation in which these regions are more disordered. Alternatively, a different number of conformationally restrained water molecules may be "released" or "acquired" between the binary AAC−aminoglycoside complex and the ternary AAC−CoASH−aminoglycoside complex, which contributes differentially to the overall entropy of the system. An increase in favorable enthalpy suggests that either a greater number of interactions of aminoglycosides with the enzyme, interactions of ligands with each other, or both are contributing to the observed increase in favorable enthalpy (more negative ΔH). The presence of both substrates in the active site is likely to be coupled to loop stabilization as undoubtedly more interactions would be required in such a conformational state. Such hypotheses are supported by the significant (5−20-fold) increase in the affinity of aminoglycoside for AAC when the CoASH binding site is saturated as observed in both ITC and fluorescence experiments (see below) (Figure 4). Significant affinity enhancements via the coenzyme have been observed for other acetyltransferases, including the aminoglycoside acetyltransferase (6′)-Iy [AAC(6′)-Iy] (*27*) and the arylalkylamine *N*-acetyltransferase (*28*), while only slight increases have been reported for the nucleotide utilizing enzymes APH (3′)-IIIa and ANT (2″)-Ia (*7*, *9*). Again, these observations suggest that thermodynamics of the enzymes that modify the central 2-DOS ring of aminoglycosides are different from those of other AGMEs.

Binding of neomycin, paromomycin, and kanamycin A to AAC was also studied by fluorescence spectroscopy (Figure 4). These studies yield dissociation constants very similar to those determined by ITC for neomycin and paromomycin (1.0 ± 0.1 and 22 ± 5 μM, respectively) and an even weaker K_D (~120 μM) for kanamycin A, confirming ITC data. We note that the change in fluorescence intensity was 11−14% for binding of neomycin and paromomycin but only ~5% for kanamycin A in binary titrations. Data acquired by fluorescence spectroscopy showed that titration of an antibiotic into the AAC−CoASH complex results in a 2−10-fold increase in aminoglycoside affinity relative to that in the respective binary titration (Figure 4). Data, fit to a single binding site, yielded dissociation constants of 0.7 ± 0.2, 3.1 ± 0.5, and 40 ± 4 μM for neomycin, paromomycin, and kanamycin A, respectively. These are in excellent agreement with those determined by ITC (Table 2).

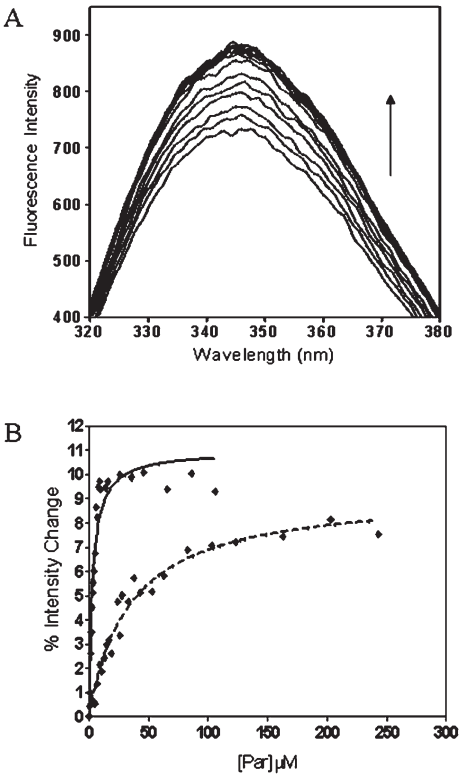

FIGURE 4: Fluorescence spectroscopy for association of an antibiotic with AAC. (A) Typical fluorescence spectrum for an antibiotic binding to AAC. As indicated by the arrow, an increase in fluorescence intensity is observed as a result of antibiotic binding. (B) Effect of CoASH on antibiotic binding. The solid and dashed curves represent one-site binding for interaction of an antibiotic with AAC in the presence and absence of the CoASH, respectively.

Unlike kinetic data where k_{cat} values of neomycins as a group were lower than those of kanamycins, there is no thermodynamic parameter that separates kanamycins from neomycins. Nor is there any correlation between the kinetic parameters K_m, k_{cat}, and k_{cat}/K_m and the thermodynamic parameters K_D, ΔH, $T\Delta S$, or ΔG for binding of aminoglycoside to AAC. However, recall in kinetic experiments that the degree of substrate inhibition is correlated with the size of the antibiotic. ITC experiments show the same size-specific trend in terms of binding stoichiometry. Binary enzyme−aminoglycoside complexes with the smaller antibiotics show a stoichiometry of 1.5−2 aminoglycoside molecules per enzyme, excluding kanamycin A, which yielded a stoichiometry of 2.8 based on data with a low signal-to-noise ratio. All larger antibiotics, including the four-ring neomycin and paromomycin as well as lividomycin with five rings, maintain N values close to 1 (Table 2).

Attempts to fit the data to a sequential binding model did not yield acceptable results. Although the crystal structure of this enzyme is not available, the computationally derived homology model of AAC predicts that the size exclusion phenomenon may be attributed to a deep cleft serving as the AG binding pocket and a gatelike loop that, on the basis of structural homology, is part of the GNAT-conserved motif B that aids acetyl acceptor binding (Figure 5). Examination of the structure and manual docking of neomycin into this pocket shows residues with negatively charged side chains in reasonable positions to interact with amine groups

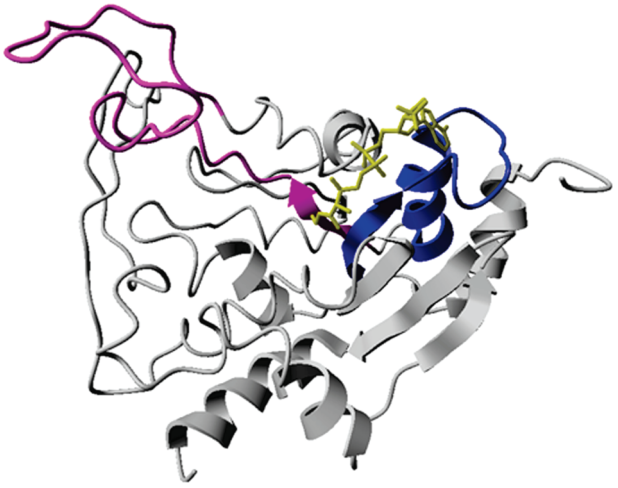

FIGURE 5: Homology model of AAC. CoASH is shown as yellow sticks and is positioned from the superpositioning of the AAC homology model with the X-ray crystal structure of AAC (3) from *Bacillus* (PDB entry 3IJW) cocrystallized with CoASH. GNAT-conserved motifs A and B are colored blue and purple, respectively.

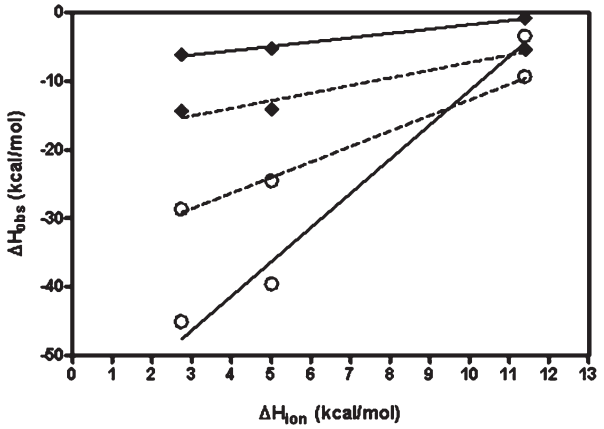

FIGURE 6: Determination of the intrinsic enthalpy of binding. The observed enthalpy of binding determined in different buffers is plotted vs the heat of ionization of the buffer as described in Experimental Procedures. The solid black lines depict data from kanamycin B in the absence (◆) and presence (○) of CoASH. Dashed lines represent the same titrations for paromomycin. R^2 values for the linear regressions are > 0.95.

of the antibiotic. These interactions would place the N-3 amine at a position proximal to the likely position of the acetyl moiety of acetyl coenzyme A based upon the homologous position of CoASH in crystal structures of both the Yokd and AAC (3) proteins from *Bacillus* (PDB entries 2NYG and 3IJW, respectively). Moreover, this proposed orientation of neomycin would allow an amine of ring D to attract a carboxyl side chain of the motif B loop, pulling it down over the active site and thus blocking any other antibiotics from entering. Manual modeling of kanamycin A into the active site shows similar interactions for the orientation of N-3. However, kanamycin A has only three rings, and the third ring does not appear to be able to interact as favorably with the gating loop. Because loops are often the most dynamic of all secondary structural elements, it is possible that this weaker antibiotic−loop association would leave the antibiotic site more exposed, thus allowing smaller aminoglycosides to bind more than one molecule at a time. It is possible that smaller aminoglycosides with relatively weak affinity for the enzyme may bind to the larger binding site in multiple orientations, leaving room for another to bind in some cases, which may explain the stoichiometry of 1.5 determined with kanamycin B and tobramycin. In this analysis, we used the experimentally determined, enzyme-bound conformation of kanamycin (*11*) which shares a common conformational motif with a number of aminoglycoside antibiotics (including neomycin) bound to several different AGMEs (*11*, *29*−*32*).

Titration of an antibiotic into an AAC−CoASH complex where only the high-affinity CoASH site is filled [described in the following paper (DOI 10.1021/bi1001568)] yields a 5−12-fold increase in antibiotic affinity. Furthermore, the binding enthalpy becomes significantly more favorable (Figures 2 and 3) while the entropic contribution becomes more disfavored. Under these conditions, the stoichiometry of binding of all aminoglycosides to the enzyme is 1/1 mol/mol regardless of their size, with the exceptions of the very weak binding butirosin, amikacin, and kanamycin A (Table 2). If the same experiment is performed under conditions where both coenzyme sites are saturated, antibiotic affinity decreases slightly while ΔH becomes less favored by 7−17 kcal/mol and $T\Delta S$ more favored by 8−17 kcal/mol relative to the conditions where only the first site is saturated. The reduced antibiotic affinity is likely the result of competition with the secondary coenzyme molecule. A calculation of the thermodynamic cycle mathematically supports the competition (Figure S2 of the Supporting Information).

These observations suggest several possibilities. First, there may be a conformational change in the protein upon coenzyme binding to the first site that prevents more than one antibiotic from coming into the active site regardless of size. Another probable situation is that CoASH binds to only one of several rapidly interconverting conformations of AAC, whereby the CoASH-bound conformation becomes the major species via a shift in equilibrium and has the loops in the proper orientation to only allow one antibiotic molecule into the binding pocket. Alternatively, the site for the second aminoglycoside may partially overlap with the first CoASH binding site, and thus, the binding of the second antibiotic molecule is prevented when CoASH has saturated this site. Further experimentation is needed to elucidate the effects of ligands on AAC structure and is beyond the scope of this work.

Role of Antibiotic Functional Groups in Binding to AAC. Binding of aminoglycosides to AAC causes changes in the pK_a values of several functional groups both in the binary and in the ternary complexes of all aminoglycosides, with the possible exception of kanamycin A in the binary complex, yielding a net protonation with the formation of each complex [$\Delta n > 0$ (Table 2)]. Determined Δn values varied between 0.4 and 1.9 for different complexes (Figure 6). Most of this represents a shift to higher pK_a values for amine functional groups in enzyme-bound aminoglycosides. However, contributions of other groups on the enzyme cannot be excluded. Such a situation has already been encountered with APH (3′)-IIIa where up- and downshifts in pK_a values of multiple functional groups both on the ligand and on the enzyme coincidentally counterbalanced each other and yielded a net value of ~0 for Δn (*5*). Thus, data interpretation, purely based on the value of Δn, can be misleading.

Binding data from both ITC and fluorescence reveal that the possession of an amine at the 2′-carbon (Figure 1) is highly favored over a hydroxyl group since kanamycin A shows the weakest dissociation constant among the antibiotics that are substrates of this enzyme (Table 2). This is consistent with the

kinetic data in which the K_m for kanamycin A is the highest of all antibiotics showing measurable rates. The importance of amine groups for aminoglycoside recognition by modifying enzymes has been observed previously (*9*, *27*, *33*−*35*). A preference for a 2′-amine occurs with AAC (6′)-Iy (*27*), APH (3′)-IIIa (*7*, *33*, *34*), and ANT (2″)-Ia (*9*). Moreover, these enzymes and AAC share the preference for 6′-amines over hydroxyls. On the basis of the few crystal structures available for AGMEs, these phenomena are likely due to the presence of carboxyl side chains of amino acids near the active site. Indeed, the homology model has several E/D residues localized on or nearby the putative antibiotic binding loop in the conserved GNAT motif B.

Although the presence of an amine group is preferred over a hydroxyl at the 6′-site, this is true only for those aminoglycosides that are equal in size (i.e., neomycin vs paromomycin) (Figure 1 and Table 2). There also appears to be a link between the size of the antibiotic and its affinity for AAC, which can take precedence over the preference for an amine group at the 6′-site. Lividomycin and ribostamycin also possess 6′-amines (Figure 1) but demonstrate a weaker affinity than neomycin. This suggests that an antibiotic too large or too small counteracts the favorable effect of the 6′-amine. The trend also holds for kanamycin class aminoglycosides where all have an NH_2 group at the 6′-carbon but consist of only three pseudosaccharide rings, causing a relative decrease in affinity as compared to those with four rings. Similar comparison, however, to determine whether the size preference can also override the preference for an amine group at the 2′-site could not be performed because of the unavailability of appropriate aminoglycoside derivatives.

Family Origins and Homology Modeling. To the best of our knowledge, all aminoglycoside acetyltransferases studied to date fall into the GNAT (GCN5-like acetyltransferase) superfamily. Proteins in this superfamily share a highly conserved structural fold despite sequence identities as low as 3% (*16*, *36*). This GNAT "core" structure is characterized by a six- or seven-strand, mixed polarity β-sheet and four conserved motifs; A, B, C, and D. Motif A is responsible for coenzyme binding, while motif B maintains a large loop region tentatively assigned to binding to the acetyl acceptor. It is thought that motif B is the source for the high degree of structural homology yet diverse acetyl transfer functionality within the GNAT superfamily (*36*).

BLAST (*37*) searches of the AAC sequence did not yield hits to any known GNAT protein. Instead, strong primary structure identity matches arise with other AAC-type proteins in *Pseudomonas aeruginosa* suggesting potential gene duplication. A variety of other bacteria also have proteins that share considerable identities and similarities to AAC. Of these, AAC (3) from *Bacillus anthracis* and Yokd from *Bacillus subtilis* have available crystal structures in the Protein Data Bank (entries 3IJW and 2NYG, respectively). COBALT sequence alignments (*38*) reveal that these two proteins are >53% identical in sequence and >72% similar to each other overall. Their crystal structures are also strikingly similar. When aligned with AAC, all three are ~20% identical and ~62% similar in terms of primary structure.

The homology model of AAC was determined as described in Experimental Procedures and is shown in Figure 5. In this model, the secondary structure is made up of 23% α-helices, 14% β-strands, 9.1% turns, and 54% random coils. Circular dichroism experiments, analyzed via CDPro (*39*), provide general support for this with 8.3% α-helix, 32.7% β-strand, 21% turn, and 38% random coil content.[2] The most striking consistency is the amount of random coils and turns, where the totals from both methods are roughly 60%. These are consistent with the experimentally detected dynamic properties of the enzyme in NMR (nuclear magnetic resonance) studies (data not shown). Such inherent flexibility may be responsible for AAC's ability to bind a number of aminoglycosides with varying structures. In this respect, AAC is like APH (3′)-IIIa which also has a very broad substrate specificity (*26*) and is an unusually flexible molecule in solution such that the apo form of this 31 kDa enzyme can exchange all of the amide protons in solution (*4*). This may be common to the most promiscuous AGMEs.

The presence of a six-strand, mixed polarity β-sheet indicates that AAC maintains the GNAT core fold. Of the four conserved GNAT motifs, only A and B could be distinguished, and each of these motifs incorporates one strand into the central β-sheet. Figure 5 shows the homology model with motifs A and B colored blue and purple, respectively, and the approximate position of coenzyme A as derived from superpositioning of the AAC (3) crystal structure from *Bacillus* that was cocrystallized with CoASH. These motifs are in structural positions homologous to those of other GNAT proteins, although the central β-strands of GNAT proteins that are side by side in the sheet are also in direct N- to C-terminal amino acid order. However, juxtaposed β-strands in AAC as well as AAC (3) and Yokd from *Bacillus* do not follow the primary sequence. Reasons for this are unclear at present.

Taken together, these data suggest that AAC (3)-IIIb is a member of the GNAT superfamily, but the homology model and crystal structures of Yokd and AAC (3) from *Bacillus* may represent a unique branch of the GNAT family fold.

CONCLUSIONS

This work represents the first thermodynamic and kinetic characterization of an aminoglycoside acetyltransferase enzyme that modifies the common 2-DOS of aminoglycoside antibiotics. Because of this specificity, AAC (3)-IIIb is a protein that is capable of conferring resistance against a large repertoire of aminoglycoside antibiotics, making it an important factor in understanding antibiotic resistance mechanisms. Thermodynamics of AGME−aminoglycoside interactions are paramount to the understanding of the molecular basis of drug−enzyme association and form a foundation for a more rational drug design to combat antibiotic resistance.

N-1-substituted aminoglycosides have the weakest affinity for AAC and are not substrates of this enzyme. AAC shows a preference for amines at 2′- and 6′-carbons, an apparently common property for most AGMEs studied to date. However, unlike other AGMEs, this preference appears to be secondary to the size preference of AAC for aminoglycosides. Furthermore, catalysis rates are strongly influenced by the chemical structure of the antibiotic, where the neomycin class being 4,5-disubstituted on the 2-DOS ring has a k_{cat} slower than that of the kanamycins 4,6-disubstiuted on 2-DOS (Figure 1). Also, small antibiotic substrates have the capacity to bind to AAC with a stoichiometry of 1.5−2.0 in the absence of the coenzyme. These same antibiotics are the only ones capable of substrate inhibition of AAC activity.

Aminoglycoside interactions occur with a favorable enthalpy and unfavorable enthalpy with an overall negative ΔG. In the presence of coenzyme, the enthalpy becomes 1.7−10.0-fold more favorable while the entropy becomes less favorable by 2.0−22.5-fold and ΔG is only more negative in the ternary complex by

[2]A. L. Norris and E. H. Serpersu, unpublished data, 2009.

1.0−1.9 kcal/mol. The affinity of aminoglycosides also increases significantly when the coenzyme is present with AAC. Note that the relationship between free energy and affinity is $\Delta G = -RT \ln(K_A)$, and thus, even the largest change in affinity, 22-fold, from binary and ternary complexes is accompanied by a 1.9 kcal/mol change in free energy.

The homology model suggests AAC is a member of the GNAT family and shows a series of loops confirmed by circular dichroism that may represent flexibility as the key to substrate promiscuity of this and other AGMEs with large substrate profiles.

SUPPORTING INFORMATION AVAILABLE

ITC data for determination of the dissociation constant of neomycin via ribostamycin competition (Figure S1) and the thermodynamic cycle of competition of a secondary CoASH with an antibiotic (Figure S2). This material is available free of charge via the Internet at http://pubs.acs.org.

REFERENCES

1. Spotts, C. R., and Stanier, R. Y. (1961) Mechanism of Streptomycin Action on Bacteria: Unitary Hypothesis. *Nature 192*, 633–637.
2. Moazed, D., and Noller, H. F. (1987) Interaction of Antibiotics with Functional Sites in 16s Ribosomal-RNA. *Nature 327*, 389–394.
3. Shaw, K. J., Rather, P. N., Hare, R. S., and Miller, G. H. (1993) Molecular Genetics of Aminoglycoside Resistance Genes and Familial Relationships of the Aminoglycoside-Modifying Enzymes. *Microbiol. Rev. 57*, 138–163.
4. Norris, A. L., and Serpersu, E. H. (2009) NMR Detected Hydrogen-Deuterium Exchange Reveals Differential Dynamics of Antibiotic- and Nucleotide-Bound Aminoglycoside Phosphotransferase 3′-IIIa. *J. Am. Chem. Soc. 131*, 8587–8594.
5. Ozen, C., Malek, J. M., and Serpersu, E. H. (2006) Dissection of aminoglycoside-enzyme interactions: A calorimetric and NMR study of neomycin B binding to the aminoglycoside phosphotransferase(3′)-IIIa. *J. Am. Chem. Soc. 128*, 15248–15254.
6. Ozen, C., Norris, A. L., Land, M. L., Tjioe, E., and Serpersu, E. H. (2008) Detection of specific solvent rearrangement regions of an enzyme: NMR and ITC studies with aminoglycoside phosphotransferase(3′)-IIIa. *Biochemistry 47*, 40–49.
7. Ozen, C., and Serpersu, E. H. (2004) Thermodynamics of aminoglycoside binding to aminoglycoside-3′-phosphotransferase IIIa studied by isothermal titration calorimetry. *Biochemistry 43*, 14667–14675.
8. Wright, E., and Serpersu, E. H. (2005) Enzyme-Substrate Interactions with an Antibiotic Resistance Enzyme: Aminoglycoside Nucleotidyltransferase-(2″)-Ia Characterized by Kinetic and Thermodynamic Methods. *Biochemistry 44*, 11581–11591.
9. Wright, E., and Serpersu, E. H. (2006) Molecular Determinants of Affinity for Aminoglycoside Binding to the Aminoglycoside Nucleotidyltransferase(2″)-Ia. *Biochemistry 45*, 10243–10250.
10. Davies, J. E. (1991) Aminoglycoside-Aminocyclitol Antibiotics and Their Modifying Enzymes. In Antibiotics in Laboratory Medicine (Lorian, V., Ed.) 4th ed., p 1283, Lippincott Williams & Wilkins, Baltimore.
11. Owston, M. A., and Serpersu, E. H. (2002) Cloning, overexpression, and purification of aminoglycoside antibiotic 3-acetyltransferase-IIIb: Conformational studies with bound substrates. *Biochemistry 41*, 10764–10770.
12. Wu, L. Z., and Serpersu, E. H. (2009) Deciphering Interactions of the Aminoglycoside Phosphotransferase(3′)-IIIa with its Ligands. *Biopolymers 91*, 801–809.
13. Atha, D. H., and Ackers, G. K. (1974) Calorimetric determination of the heat of oxygenation of human hemoglobin as a function of pH and the extent of reaction. *Biochemistry 13*, 376–23822.
14. Williams, J. W., and Northrop, D. B. (1978) Kinetic Mechanisms of Gentamicin Acetyltransferase-I - Antibiotic-Dependent Shift from Rapid to Nonrapid Equilibrium Random Mechanisms. *J. Biol. Chem. 253*, 5902–5907.
15. Lambert, C., Leonard, N., De Bolle, X., and Depiereux, E. (2002) ESyPred3D: Prediction of proteins 3D structures. *Bioinformatics 18*, 1250–1256.
16. Arnold, K., Bordoli, L., Kopp, J., and Schwede, T. (2006) The SWISS-MODEL workspace: A web-based environment for protein structure homology modelling. *Bioinformatics 22*, 195–201.
17. Kiefer, F., Arnold, K., Künzli, M., Bordoli, L., and Schwede, T. (2009) The SWISS-MODEL Repository and associated resources. *Nucleic Acids Res. 37*, D387–D392.
18. Peitsch, M. C. (1995) Protein Modeling by E-mail. *Nat. Biotechnol. 13*, 658–660.
19. Combet, C., Jambon, M., Deleage, G., and Geourjon, C. (2002) Geno3D: Automatic comparative molecular modelling of protein. *Bioinformatics 18*, 213–214.
20. Molecular Operating Environment, Chemical Computing Group Inc., Montreal (http://www.chemcomp.com).
21. Kim, C., Hesek, D., Zajicek, J., Vakulenko, S. B., and Mobashery, S. (2006) Characterization of the bifunctional aminoglycoside-modifying enzyme ANT(3″)-Ii/AAC(6′)-IId from *Serratia marcescens*. *Biochemistry 45*, 8368–8377.
22. Toth, M., Zajicek, J., Kim, C., Chow, J. W., Smith, C., Mobashery, S., and Vakulenko, S. (2007) Kinetic mechanism of enterococcal aminoglycoside phosphotransferase 2″-Ib. *Biochemistry 46*, 5570–5578.
23. Magalhaes, M. L. B., and Blanchard, J. S. (2005) The kinetic mechanism of AAC(3)-IV aminoglycoside acetyltransferase from *Escherichia coli*. *Biochemistry 44*, 16275–16283.
24. Draker, K. A., Northrop, D. B., and Wright, G. D. (2003) Kinetic mechanism of the GCN5-related chromosomal aminoglycoside acetyltransferase AAC(6′)-Ii from *Enterococcus faecium*: Evidence of dimer subunit cooperativity. *Biochemistry 42*, 6565–6574.
25. Badarau, A., Shi, Q., Chow, J. W., Zajicek, J., Mobashery, S., and Vakulenko, S. (2008) Aminoglycoside 2″-phosphotransferase type IIIa from *Enterococcus*. *J. Biol. Chem. 283*, 7638–7647.
26. McKay, G. A., Thompson, P. R., and Wright, G. D. (1994) Broad spectrum aminoglycoside phosphotransferase type III from *Enterococcus*: Overexpression, purification and substrate specificity. *Biochemistry 33*, 6936–6944.
27. Hedge, S. S., Dam, T. K., Brewer, C. F., and Blanchard, J. S. (2002) Thermodynamics of aminoglycoside and acyl-coenzyme A binding to the *Salmonella enterica* AAC(6′)-Iy aminoglycoside N-acetyltransferase. *Biochemistry 41*, 7519–7527.
28. De Angelis, J., Gastel, J., Klein, D. C., and Cole, P. A. (1998) Kinetic analysis of the catalytic mechanism of serotonin N-acetyltransferase (EC 2.3.1.87). *J. Biol. Chem. 273*, 3045–3050.
29. Cox, J. R., and Serpersu, E. H. (1997) Biologically important conformations of aminoglycoside antibiotics bound to an aminoglycoside 3′-phosphotransferase as determined by transferred nuclear Overhauser effect spectroscopy. *Biochemistry 36*, 2353–2359.
30. DiGiammarino, E. L., Draker, K., Wright, G. D., and Serpersu, E. H. (1998) Solution studies of isepamicin and conformational comparisons between isepamicin and butirosin A when bound to an aminoglycoside 6′-N-acetyltransferase determined by NMR spectroscopy. *Biochemistry 37*, 3638–3644.
31. Ekman, D. R., DiGiammarino, E. L., Wright, E., Witter, E. D., and Serpersu, E. H. (2001) Cloning, overexpression, and purification of aminoglycoside antibiotic nucleotidyltransferase (2″)-Ia: Conformational studies with bound substrates. *Biochemistry 40*, 7017–7024.
32. Serpersu, E. H., Cox, J. R., DiGiammarino, E. L., Mohler, M. L., Ekman, D. R., Akal-Strader, A., and Owston, M. (2000) Conformations of antibiotics in active sites of aminoglycoside-detoxifyiing enzymes. *Cell Biochem. Biophys. 33*, 309–321.
33. Roestamadji, J., Grapsas, I., and Mobashery, S. (1995) Loss of Individual Electrostatic Interactions between Aminoglycoside Antibiotics and Resistance Enzymes as an Effective Means to Overcoming Bacterial Drug Resistance. *J. Am. Chem. Soc. 117*, 11060–11069.
34. McKay, G. A., Roestamadji, J., Mobashery, S., and Wright, G. D. (1996) Recognition of aminoglycoside antibiotics by enterococcal-staphylococcal aminoglycoside 3′-phosphotransferase type IIIa: Role of substrate amino groups. *Antimicrob. Agents Chemother. 40*, 2648–2650.
35. Gates, C. A., and Northrop, D. B. (1988) Substrate Specificities and Structure Activity Relationships for the Nucleotidylation of Antibiotics Catalyzed by Aminoglycoside Nucleotidyltransferase-2″-I. *Biochemistry 27*, 3820–3825.
36. Dyda, F., Klein, D. C., and Hickman, A. B. (2000) GCN5-related N-acetyltransferases: A structural overview. *Annu. Rev. Biophys. Biomol. Struct. 29*, 81–103.
37. Altschul, S. F., Gish, W., Miller, W., Myers, E. W., and Lipman, D. J. (1990) Basic Local Alignment Search Tool. *J. Mol. Biol. 215*, 403–410.
38. Papadopoulos, J. S., and Agarwala, R. (2007) COBALT: Constraint-based alignment tool for multiple protein sequences. *Bioinformatics 23*, 1073–1079.
39. Sreerama, N., Venyaminov, S. Y., and Woody, R. W. (1999) Estimation of the number of α-helical and β-strand segments in proteins using circular dichroism spectroscopy. *Protein Sci. 8*, 370–380.